Environmental Science & Technology

pubs.acs.org/est

Article

Mass-Independent Fractionation of Mercury Isotopes during Photoreduction of Soot Particle Bound Hg(II)

Qiang Huang, Xiaoshuai He, Weilin Huang, and John R. Reinfelder*

Cite This: *Environ. Sci. Technol.* 2021, 55, 13783−13791

Read Online

ACCESS | Metrics & More | Article Recommendations | Supporting Information

ABSTRACT: Soot and mercury (Hg) are two notorious air pollutants, and the fate and transport of Hg may be affected by soot at various scales in the environment as soot may be both a carrier and a reactant for active Hg species. This study was designed to quantify photoreduction of Hg(II) in the presence of soot and the associated Hg isotope fractionation under both atmospheric aerosol and aqueous conditions (water-saturated). Photoreduction experiments were conducted with diesel soot particulate matter under controlled temperature and relative humidity (RH) conditions using a flow-through semibatch reactor system. Mass-dependent fractionation resulted in the enrichment of heavier Hg isotopes in the remaining Hg(II) with enrichment factors (ε^{202}Hg) of 1.48 ± 0.02‰ (±2 standard deviation) to 1.75 ± 0.05‰ for aerosol-phase reactions (RH 28−68%) and from 1.26 ± 0.11 to 1.50 ± 0.04‰ for aqueous-phase reactions. Positive odd mass-independent fractionation (MIF) was observed in aqueous-phase reactions, resulting in Δ^{199}Hg values for reactant Hg(II) as high as 5.29‰, but negative odd-MIF occurred in aerosol-phase reactions, in which Δ^{199}Hg values of reactant Hg(II) varied from −1.02 to 0‰. The average ratio of Δ^{199}Hg/Δ^{201}Hg (1.1) indicated that under all conditions, MIF was dominated by magnetic isotope effects during photoreduction of Hg(II). Increasing RH resulted in higher reduction rates but lower extents of negative MIF in the aerosol-phase experiments, suggesting that the reduction of soot particle-bound Hg(II) was responsible for the observed negative odd-MIF. Our results suggest that mass-independent Hg isotope fractionation during Hg(II) photoreduction varies with soot aerosol water content and that Hg-stable isotope ratios may be used to understand the transformational histories of aerosol-bound Hg(II) in the environment.

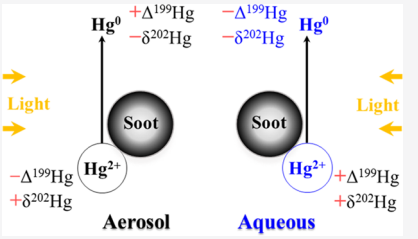

KEYWORDS: *mercury, mass-independent fractionation, aerosol photoreaction, relative humidity, magnetic isotope effects*

1. INTRODUCTION

Redox transformations of mercury (Hg) are of major importance to the regional distribution and global geochemical cycling of Hg through their influence on atmospheric Hg deposition and re-emission from surface environments. Photoreduction of Hg(II) takes place in aerosols and clouds,[1] where high irradiance and large aerosol surface areas are available for physicochemical interactions among gaseous and particulate-bound species.[2] Indeed, Hg(II) photoreduction in aerosols has been observed in controlled laboratory experiments[3,4] and in the environment.[5,6] Although the effects of aerosol chemical composition (e.g., anions, trace elements, and carbon concentrations) and water content on Hg(II) photoreduction have been examined,[3,4] due to the complexity of aerosols in the environment, the heterogeneous chemistry of Hg(II) in the atmosphere is not well-understood and the impact of photoreduction on the fate of Hg in the environment has not been fully assessed.[7]

As one of the major components of urban air pollution, soot is an efficient sorbent for various environmental pollutants due to its surface structure and unique physicochemical properties,[8] which facilitates multiphase photochemical processes through direct reactions with other species or as a catalytic surface.[9] Prior studies have shown that soot plays an important role in photochemical reactions not only in clouds and aerosols[9−11] but also in aquatic environments including marine surface waters.[11] While the results of laboratory and field studies show that elemental carbon particles have a high capacity to adsorb Hg, especially Hg(II), in the atmosphere,[12] the role of soot in the photochemical transformation of Hg in the atmosphere is unknown.

This study was designed to quantify the effects of soot on the photoreduction and isotope fractionation of Hg in the atmosphere. Stable isotopes of Hg exhibit both mass-dependent fractionation (MDF, represented by δ^{202}Hg) and mass-independent fractionation (MIF) during Hg transformations under various environmental conditions.[13−19] MIF includes odd-mass-number MIF (odd-MIF), represented by Δ^{199}Hg and Δ^{201}Hg, and even-mass-number MIF (even-MIF), represented by Δ^{200}Hg and Δ^{204}Hg. Prior studies have shown that MDF is induced by several Hg transformation and

Received: April 23, 2021
Revised: September 23, 2021
Accepted: September 24, 2021
Published: October 8, 2021

https://doi.org/10.1021/acs.est.1c02679
Environ. Sci. Technol. 2021, 55, 13783−13791

transport processes,[15,20−28] but large values of odd-MIF result primarily from photochemical reactions under various environmental conditions.[15,29,30]

Variations in Hg-stable isotope ratios have been used to trace reactions of Hg in the environment and to track sources of Hg in food webs and across boundaries of atmospheric and aquatic systems.[31,32] Previous results show that Hg-stable isotope ratios in atmospheric fine particles were correlated with elemental carbon concentrations[33] and that photochemical reactions cause major daily swings in MDF and MIF of Hg isotopes in urban fine aerosols.[5] However, the patterns and environmental controls of Hg isotope fractionation in aerosols are still not clear. Indeed, Hg isotope ratios of aerosols are typically explained as being controlled by aqueous-phase photoreduction.[5,34−36] Such practice is predicated on the hypotheses that photoreduction of Hg(II) would follow the same reaction mechanisms and similar Hg isotope fractionation patterns in both aerosol and aqueous phases.

We tested the abovementioned hypotheses regarding Hg photoreduction in a laboratory study with both dry aerosol and aqueous phases. Atmospheric photoreduction of Hg was examined under controlled temperature and relative humidity (RH) conditions using a flow-through, semibatch reactor system with diesel soot particulate matter (DSPM) as the stationary phase and an inert gas (argon) as the mobile phase. For comparison, aqueous-phase experiments were also conducted with DSPM suspensions and filtrates. We refer to the filtrate of DSPM as water-soluble diesel soot (WSDS) due to the dissolution of soot fractions including macromolecular humic-like substances and aromatic polyacids,[37,38] which may act like dissolved organic carbon with respect of Hg isotope fractionation during Hg photoreduction.[39] We expected isotope fractionation of Hg during photoreduction of soot-bound Hg(II) to follow the same patterns in both aerosol and aqueous phases. Our aims were therefore to (1) determine the rate of photoreduction of Hg(II) bound to DSPM in the aerosol phase at four different RHs and in aqueous systems with DSPM suspensions and filtrates (WSDS) and (2) investigate Hg isotope fractionation during Hg photoreduction in aerosol and aqueous phases. Our results illustrate the effects of RH on the photochemical reduction of soot-bound Hg and show that the direction of odd-MIF of Hg isotopes depends on whether reactions occur in aerosol or aqueous phases.

2. EXPERIMENTAL SECTION

Reagents, Chemicals, and Solutions. Mercury chloride ($HgCl_2$, >99.5%, Alfa Aesar), stannous chloride ($SnCl_2{\cdot}2H_2O$, 98.0−103.0%, Alfa Aesar), hydroxylammonium chloride ($NH_2OH{\cdot}HCl$, >99.0%, Sigma-Aldrich), potassium bromide (KBr, >99.0%, Sigma-Aldrich), and potassium bromate ($KBrO_3$, >99.8%, Sigma-Aldrich) were all of ACS reagent grade. Trace metal-grade nitric acid (HNO_3) and hydrochloric acid (HCl) were purchased from Fisher Scientific. Ultrapure water (18.2 MΩ cm) through a Barnstead water purification system was used for preparing all solutions with precleaned glassware. A standard reference material of DSPM (SRM 2975) was purchased from The National Institute of Standards and Technology (NIST). The NIST SRM 2975 has been well-characterized and widely used as a representative soot particulate matter in prior studies of pollutant fate and transport under atmospheric or aquatic conditions.[8,40] Briefly, its certified characteristics include a mean diameter of 1.62 ± 0.01 μm (number distribution), a specific surface area of 114 m^2/g, an extractable organic material of 6.0 wt %, an elemental carbon content of 75.0 wt %, and a total carbon content of 89.5 wt %.[8]

A bromine chloride (BrCl) solution (0.2 M) was prepared by mixing concentrated HCl (11.3 M) with prebaked (250 °C, 12 h) KBr and $KBrO_3$ powders. Aqueous $SnCl_2$ solutions at both 100 and 30 g/L used for on-line reduction of Hg(II) for concentration and isotope analyses, respectively, were prepared by dissolving the solid in 1 M HCl. A 100 g/L $NH_2OH{\cdot}HCl$ solution was prepared for BrCl neutralization. Before use, the $SnCl_2$ and $NH_2OH{\cdot}HCl$ solutions were bubbled for 6 h with Hg-free N_2 to remove trace levels of Hg vapor. A stock solution of $HgCl_2$ (0.8 M) was prepared by dissolving the solid in 0.01 M HCl. A mixture of 4 M HNO_3 and 1.5 M HCl prepared by mixing 11.3 M HCl, 15 M HNO_3, and ultrapure water in the proportions 2:4:9 by volume was used as the trapping solution.

All glass and plastic containers and connectors used in the experiment and for sample storage and analysis were soaked with 4 M HCl solution for 1−2 days and rinsed with ultrapure water. They were air-dried in a laminar flow hood equipped with a class 100 high-efficiency particulate air filter and stored in plastic bags.

Photoreaction Systems. The rates of photoreduction of DSPM-bound Hg(II) were investigated under both aerosol and aqueous conditions using two home-made photoreaction systems. The photoreaction system for aerosol experiments was tailored specifically for carrying out the experiments using commercially available components and equipment. It is described in greater detail in the Supporting Information and is schematically shown in Figure S1. In brief, four reactors made of quartz tube (I.D. 20 mm, 150 mm length) were positioned vertically at equal distances surrounding a lamp. Each reactor was fitted with a Hg-free argon gas supply line on the bottom and outflow line to an acid trap on the top. The trapping system consisted of a 20 mL borosilicate glass culture tube (O.D. × L: 16 × 150 mm) with a screw cap, which contained 5 mL of a solution (4 M HNO_3 and 1.5 M HCl) for trapping all Hg as aqueous Hg(II) and a gas dispersion tube (height 220 mm approx., I.D. 3 mm, O.D. 6 mm) with a 12 mm-diameter coarse-porosity (20−50 μm) fritted cylinder for dispersing mercury gas in the trapping solution. The trapping method used here was adapted from a prior study which showed its high efficiency.[33] The Hg-free argon gas was used to control the humidity for the aerosol reaction and to purge Hg(0) out of the reactor. The flow was controlled by mixing a dry argon gas flow with a water-saturated argon flow which was bubbled through a water bath at room temperature (about 23 °C). For each reactor, the total inlet argon flow was set at 45 ± 1 mL/min and the desired constant humidity was achieved with two adjustable gas flow meters (Cole Parmer, USA). Simulated solar radiation was supplied using a xenon lamp with light intensities of 2600 mW/cm^2 in the visible range (400−700 nm, measured with a model LI-250 m, LI-COR, NE, USA) and 7 mW/cm^2 and 0.18 mW/cm^2 in the UV-A and UV-B ranges, respectively (PMA2200, Solar Light, PA, USA). Multiple reactors were used simultaneously to run duplicate or triplicate experiments under identical conditions. The xenon lamp was surrounded with a hollow quartz cylindrical jacket about 2 cm thick. The jacket contained 5 °C water from a recirculating chiller to absorb heat. The reactors and lamp were placed in the dark, and the lamp was the only source of light during the experiments.

https://doi.org/10.1021/acs.est.1c02679
Environ. Sci. Technol. 2021, 55, 13783−13791

For aqueous experiments, the photoreaction system consisted of a 45 mL quartz reactor with a gas outlet and a fritted cylinder of 12 mm diameter and coarse porosity (20−50 μm) as the gas inlet, and the same xenon lamp as was used in the aerosol system. Water-saturated argon gas was used for purging, and a trapping system identical to that in the aerosol system was connected to the gas outlet. Both photoreaction systems were kept in the dark, so the xenon lamp was the only source of light.

Photoreaction Experiments. A DSPM suspension stock solution at 2.79 mg/mL was prepared by suspending DSPM in ultrapure water. A fraction of the stock solution was filtered through a 0.2 μm cellulose membrane filter (4 mm, Corning syringe filter, Sigma-Aldrich) and the filtrate having a WSDS carbon content of 13.1 μg/mL was retained for aqueous-phase photoreduction tests. Both the DSPM and WSDS solutions were stored in 20 mL brown glass bottles at 5 °C before use. Before each photoreduction test, 0.50 mL of Hg(II)-DSPM or Hg(II)-WSDS solution was prepared by mixing 0.01 mL of $HgCl_2$ working solution (164 μg/mL of Hg) with 0.49 mL of DSPM or WSDS solution, yielding a final Hg/C molar ratio of 7.8×10^{-5} or 1.5×10^{-2}. The Hg(II) mixture was ultrasonically agitated for 15 s and then placed on a shaker at 150 rpm for 15 min. After mixing, an aliquot (50 μL) of the Hg(II)-DSPM was sampled and filtered, and the filtrate was analyzed for the concentration of dissolved Hg(II). The results showed that less than 5% of the total Hg introduced to the DSPM suspension was in the dissolved phase, indicating that nearly all of the Hg(II) was bound to DSPM.

For aerosol experiments, 100 μL of a Hg(II)-DSPM suspension was transferred with a pipette and spread evenly over the entire frosted surface of a quartz plate (17 × 100 mm). After being dried in a dark hood for 10 min, the plate was immediately placed into the quartz reactor with the frosted side facing the lamp. Before irradiation, the reactor was purged with Hg-free and constant-humidity argon gas for 20 min to remove any small amount of Hg(0) and to achieve equilibrated humidity. The temperature inside each reactor, which was monitored during irradiation, rose from 23 to 28 °C within the first 10 min and remained relatively constant between 28 and 30 °C thereafter. Experiments with DSPM aerosols were run at four different RH levels, 28, 48, 68, and 75%, as measured in the reactor using a digital psychrometer (RH300, Extech Instrument), which was calibrated against salt-saturated aqueous solution-vapor standards. At a designated time, the trapping unit was replaced, and the trapping solution and a water rinse were combined in a 15 mL culture tube, which was spiked with 50 μL of 0.2 M BrCl to preserve trapped Hg and sealed with a PTFE-lined cap. At the end of each experiment, the entire reactor, including the quartz plate and inside walls, was rinsed with 10 mL of trapping solution and 10 mL of ultrapure water for recovering the residual Hg in the reactor. The aliquots were combined and then spiked with 0.5 mL of 0.2 M BrCl.

For aqueous experiments, the quartz reactor contained 20 mL of ultrapure water and 100 μL of Hg(II)-DSPM or Hg(II)-WSDS, yielding a Hg concentration of 16.4 ng/mL. The contents of each treatment were allowed to equilibrate for 20 min in the dark with purging Ar gas. At this dilution, the equilibrated aqueous phase of Hg(II)-DSPM treatments accounted for about 23% of total Hg. During irradiation, the trapping unit was replaced at preset times, and trapping solutions were preserved as described above. At the end of each experiment, the remaining solution was transferred into a 50 mL glass bottle, and the reactor was rinsed with the trapping solution (10 mL). The solutions were combined and 0.5 mL of 0.2 M BrCl was added.

Dark control experiments with aluminum foil-wrapped reactors were also carried out under identical conditions. All the trapping samples and the residual samples listed in Table S1 were stored at 4 °C before subsequent analyses for Hg concentration and isotope composition.

Analytical Methods. The concentrations of Hg in all aqueous samples were measured by cold vapor atomic fluorescence spectrometry (Brooks Rand Labs MERX automated systems with Model III Atomic Fluorescence Detector) following EPA method 1631 revision E. The relative standard deviation (SD) was ≤5% based on repeated analysis of samples ($n = 4$).

A total of five sets of reaction solutions were chosen for Hg isotope measurements, two sets from aerosol experiments at an RH of 28 and 68% and three sets from aqueous experiments including one for Hg(II)-DSPM and two for Hg(II)-WSDS. The Hg isotope ratios were measured by multicollector inductively coupled plasma mass spectrometry (MC-ICPMS, Thermo Scientific Neptune Plus) at the Department of Earth and Planetary Sciences, Rutgers University, using the method described elsewhere.[41,42] In brief, 10 μL of a 100 g/L NH_2OH·HCl solution was added to all samples to neutralize excess BrCl before analysis. The MC-ICPMS was coupled to a cold vapor generation system (HGX-200, Cetac, Omaha, NE, USA), where Hg(II) was converted to Hg(0) vapor by inline mixing with a 30 g/L $SnCl_2$ solution and subsequently combined with thallium (Tl) aerosol generated using a Cetac Aridus II Desolvating Nebulizer System. Tl solution at 20 μg/L was prepared from a Tl standard (10 ppm in 2% HNO_3, Elemental Scientific), which was used for isotopic mass bias correction. Faraday cup detectors were positioned to measure five isotopes of mercury (^{198}Hg, ^{199}Hg, ^{200}Hg, ^{201}Hg, and ^{202}Hg) and two isotopes of thallium (^{203}Tl and ^{205}Tl). Mass bias was corrected using the $^{205}Tl/^{203}Tl$ internal standard and standard bracketing with a 2 μg/L Hg standard (NIST 3133). The sample was diluted to a Hg concentration of 2 μg/L and was introduced to the cold vapor generation system at 0.75 mL/min, which typically gave an instrumental sensitivity of 1.5 V on ^{202}Hg. All isotope ratios of samples and secondary standards were measured relative to NIST-3133. Results are reported as $\delta^x Hg_{NIST}$ in units of per mil (‰) as defined using the following equation

$$\delta^x Hg_{NIST}(‰) = [(^xHg/^{198}Hg)_{sample}/(^xHg/^{198}Hg)_{NIST3133} - 1] \times 1000 \quad (1)$$

where $x = 199$, 200, 201, or 202. MIF is reported as $\Delta^x Hg_{NIST}$, which is the difference between observed and theoretically predicted kinetic MDF values according to the equation

$$\Delta^x Hg_{NIST}(‰) = \delta^x Hg_{NIST} - \beta \times \delta^{202} Hg_{NIST} \quad (2)$$

where β values are 0.252, 0.5024, and 0.752 for ^{199}Hg, ^{200}Hg, and ^{201}Hg, respectively.

A well-known reference material UM-Almaden standard was regularly measured between samples and reproduced at $\delta^{202}Hg_{NIST} = -0.54 \pm 0.12‰$ and $\Delta^{199}Hg_{NIST} = -0.03 \pm 0.04‰$ (2 SD, $n = 10$), which are in agreement with published values.[33,43] Multiple measurements of the mercury (II)

https://doi.org/10.1021/acs.est.1c02679
Environ. Sci. Technol. 2021, 55, 13783−13791

chloride solution used in the reaction experiments resulted in values of $\delta^{202}Hg_{NIST}$ = −0.47 ± 0.12‰ and $\Delta^{199}Hg_{NIST}$ = −0.03 ± 0.06‰ (2 SD, n = 11). The uncertainties of isotope ratios of samples listed in Table S2 used the abovementioned 2 SD values for the laboratory $HgCl_2$ solution since the average standard error (2 SE) of samples calculated based on repeated analyses was lower than the 2 SD of the laboratory $HgCl_2$ solution.

Data Analysis. The time-dependent mass fraction (f_i) of Hg(0) formation, the accumulative mass fraction (f_P) of Hg(0) production, and the fraction (f_R) of residual reactant Hg(II) were calculated (see Table S1) based on a mass balance approach using the total Hg (Hg_{total}) of each reaction system calculated from the analyses of the purged-out mercury (Hg_i) and the residual mercury (Hg_{re}) after completion of the reaction.

$$f_P = \sum_{i=0}^{n} f_i = \sum_{i=0}^{n} (Hg_i/Hg_{total}) \quad (3)$$

The initial Hg isotope compositions of total Hg in each photoreactor (i.e., $\delta^{202}Hg_{initial}$) were calculated from measured isotope compositions of purged-out Hg(0) (i.e., $\delta^{202}Hg_i$) and residual Hg(II) present at the end of each incubation (i.e., $\delta^{202}Hg_{re}$)

$$\delta^x Hg_{initial} = \sum_{i=0}^{n} (\delta^x Hg_i \times f_i) + \delta^x Hg_{re} \times Hg_{re}/Hg_{total} \quad (4)$$

The resulting average values of $\delta^{202}Hg_{initial}$ = −0.42 ± 0.10‰ and $\Delta^{199}Hg_{initial}$ = −0.06 ± 0.10‰ (2 SD, n = 5) were consistent with the isotope compositions of the mercury(II) chloride salt ($\delta^{202}Hg$ = −0.47 ± 0.12‰ and $\Delta^{199}Hg$ = −0.03 ± 0.06‰, n = 11), indicating that preparation procedures had little or no effect on the isotope ratios of added Hg. Because the initial Hg(II) used for experiments had nonzero δ^xHg and Δ^xHg values and to simplify subsequent data analysis and presentation, Hg isotope ratios of all samples are reported relative to the isotope composition of the mercury(II) chloride salt.

The isotope ratios of cumulatively produced Hg(0) (i.e., $\delta^{202}Hg_P$) were calculated from the isotope compositions of interval samples (i.e., $\delta^{202}Hg_i$) and their fractions (f_i)

$$\delta^x Hg_p = \sum_{i=0}^{n} (\delta^x Hg_i \times f_i/f_p) \quad (5)$$

The isotopic ratios (i.e., $\delta^{202}Hg_R$) of residual reactant Hg(II) were calculated using the isotope compositions of the cumulative produced Hg(0) (i.e., $\delta^{202}Hg_P$) and their fractions (f_P)

$$\delta^x Hg_R = [(\delta^x Hg_{initial} - \delta^x Hg_{mercury(II)chloride\ salt}) \times 1 - \delta^x Hg_p \times f_p]/f_R \quad (6)$$

Calculated $\delta^x Hg_P$ and $\delta^x Hg_R$ and associated MIF values referred to in the Results and Discussion are presented in Table S3. Since our experimental design included an inert mobile phase and continuous purging to prevent Hg oxidation, kinetic isotope fractionation was examined. The kinetic fractionation factors (α) between the reactant Hg(II) and product Hg(0) are defined as $\alpha^{x/198} = R_R/R_P$, where R is the isotope ratio $^xHg/^{198}Hg$ (x = 199, 200, 201, and 202). The following equations,[44] which are based on the Rayleigh distillation model, were used to evaluate the kinetic fractionation factor of MDF

$$10^3 \times \ln[(10^3 + \delta^x Hg_R)/(10^3 + \delta^x Hg_{initial})] = (-)10^3 \times (\alpha_{MDF}{}^{x/198} - 1) \times \ln f_R \quad (7)$$

where $\delta^x Hg_{initial}$ is the calculated initial δ^xHg value of reactant Hg(II) when f_R = 1, and the slope, $(-)10^3 \times (\alpha_{MDF}x/198 - 1)$, is also defined as an enrichment factor for MDF (ε^xHg). The left side of eq 7 can be replaced with $\delta^x Hg_R$, since the initial isotope composition was normalized to zero. The enrichment factors calculated by linear regression are presented in Table S4.

QA/QC. During the photochemical experiments, Hg(II) was reduced to Hg(0), which was purged out of the reactor by argon. The Hg_{total} calculated for each run ranged from 292 to 442 ng, which equaled an average of 95 ± 6% (±1 SD, from 81 to 104%) of the total Hg estimated from the volume and the Hg concentration of the Hg(II)-DSPM solution added to each reactor. This variance likely resulted from the complex experimental procedures involved and propagation of uncertainty in Hg measurements. Nevertheless, the triplicates of each reactor system exhibited a very similar trend of photoreduction rate and consistent time-dependent changes in f_R under irradiation (see Figure S2). In dark control experiments (see Figure S2), f_R values were linearly correlated with reaction time in both aerosol and aqueous phases, and the rate of Hg(II) reduction was a factor of 5 lower than that of photoreduction over 17.5 h in aerosol-phase experiments at RH 68% and a factor of 12 lower over 10.5 h in aqueous-phase experiments with DSPM suspensions. It is likely that the dark reduction of Hg(II) might follow a zeroth-order rate model and should have limited contribution to the reduction of Hg(II) during the photoreaction.

Hg isotope values were measured for samples from five reactors, including two for aerosol experiments at an RH of 28 and 68%, respectively, and three for aqueous experiments (one Hg(II)-DSPM and two Hg(II)-WSDS systems). As shown in Figure S3, the duplicates of Hg(II)-WSDS exhibited the same pattern of Hg(II) photoreduction rates and consistent isotope fractionation trends, demonstrating experimental repeatability.

3. RESULTS AND DISCUSSION

Mercury Photoreduction Rates and Their Relationship with RH. RH had a strong effect on the photoreduction of Hg(II) with DSPM aerosols as the observed rate was clearly faster and the extent of the reaction was greater at higher humidity (Figure 1). In triplicate experiments, an average of 23 ± 4.7, 45 ± 3.3, 59 ± 1, and 66 ± 1.4% of initial Hg(II) was reduced to Hg(0) over 13 h at RH values of 28, 48, 68, and 75%, respectively. In all experiments, Hg(II) followed an exponential decline (Figure 1) and results (Table S5) were fit to a two-compartment, pseudo-first-order rate model ($0.991 < R^2 < 1.000$)

$$f_R = A \times \exp(-k_1 \times t) + (1 - A) \times \exp(-k_2 \times t) \quad (8)$$

where A and $1 - A$ are the fractions of Hg(II) in each compartment and k_1 and k_2 are their respective rate constants. A single compartment first-order model gave weaker correlations (adj R^2 < 0.98) than the two-compartment

https://doi.org/10.1021/acs.est.1c02679
Environ. Sci. Technol. 2021, 55, 13783−13791

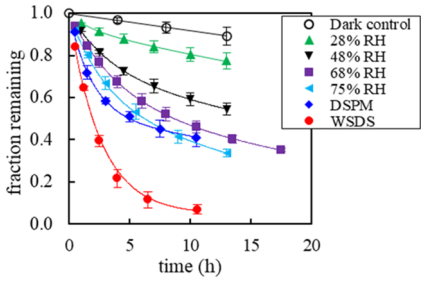

Figure 1. Photoreduction of Hg(II) with DSPM aerosols at various RHs and in aqueous-phase experiments with DSPM suspensions and filtrates (WSDS). Plotted values are the fractions of the remaining Hg(II) (f_R = 1 − $Hg_{product}/Hg_{total}$) at each time. Lines are for two-compartment, pseudo-first-order rate model fits to the results (see text). Error bars represent the range of f_R values for duplicate reactors.

model. The photoreduction of Hg(II) in compartment 1 was much faster (k_1 = 0.26 to 0.50 h^{-1}) than compartment 2 (k_2 = 0.005 to 0.047 h^{-1}). The increase in the proportion of Hg(II) in compartment 1 from 0.08 to 0.40 as RH increased therefore largely accounts for the higher rate of Hg(II) photoreduction at higher water levels. A smaller portion of this effect is due to the increase in the rate constant for the photoreduction of Hg(II) in compartment 2 (k_2) with increasing RH.

While the coordination of Hg(II) to different sites on the surface of DSPM particles could account for the presence of two different reactive forms of Hg(II), the observed increase in the rates and extents of Hg(II) photoreduction, as well as the proportion of Hg(II) in compartment 1, with higher humidity in the soot aerosol experiments suggests that compartment 1 represents water-soluble forms of soot. This hypothesis is supported by our observation of a higher rate and extent of Hg(II) photoreduction in incubations with WSDS particles in which the fast reacting compartment accounted for nearly all (95%) Hg(II) than in experiments with DSPM suspensions in which Hg(II) was evenly divided between the two compartments. The presence of suspended soot particles apparently slowed the photoreduction of Hg(II) by binding half of the Hg(II) in less-reactive compartment 2 in the aerosol experiments. Photoreduction rate constants for compartment 1 were significantly lower (p < 0.05) at intermediate RHs of 48 and 68% than those at both the lowest RH and at higher RH and in aqueous experiments. This may reflect changes in the structure of soot particle surfaces or the partitioning of Hg(II) between aqueous and particle-bound forms with different reactivities as water content increased.

Hg-Stable Isotope Fractionation. Both MDF and odd-MIF were observed in all experiments, but even-MIF was not observed within analytical uncertainty for most samples. Thus, only MDF and odd-MIF are discussed hereafter.

Hg(II) photoreduction in both aerosol- and aqueous-phase experiments exhibited MDF. Figure 2a presents the δ^{202}Hg values of both the reactant and product as a function of the remaining mass fraction of Hg(II) (f_R). Lighter Hg isotopes accumulated in product Hg(0) to a greater extent, as indicated by negative δ^{202}Hg values, and heavier Hg isotopes remained in reactant Hg(II) to a greater extent, as indicated by positive δ^{202}Hg values. The mass-dependent Hg isotope fractionation we observed in both aerosol- and aqueous-phase experiments is comparable with that in previous studies of Hg(II) photoreduction with dissolved organic matter (DOM) in aquatic systems (−0.49 ± 0.32 to −1.73 ± 0.23‰).[15,39,45]

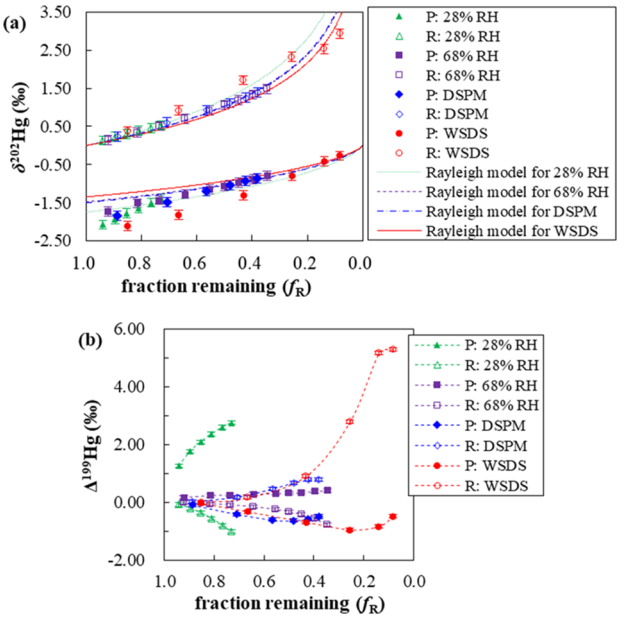

Figure 2. Fractionation of mercury-stable isotopes during photochemical reduction of Hg(II) with DSPM aerosols at two RHs and in aqueous-phase experiments with DSPM suspensions and filtrates (WSDS). (a) δ^{202}Hg values of the reactant (R) and cumulative product (P) and (b) Δ^{199}Hg values of the reactant (R) and cumulative product (P). The fractions of the remaining Hg(II) (f_R) were calculated as 1 − $Hg_{product}/Hg_{total}$.

Since product Hg(0) was instantaneously removed, isotope enrichment factors for ^{202}Hg (ε^{202}Hg) were obtained from linear regression of eq 7, assuming Rayleigh fractionation. For the aerosol experiments, the estimated reactant/product ε^{202}Hg had a slightly less positive value at an RH of 68% (1.48 ± 0.02‰, R^2 = 0.997) than at an RH of 28% (1.75 ± 0.05‰, R^2 = 0.994). The ε^{202}Hg value of Hg(II) at RH 68% was statistically very similar (p > 0.05) to that of the aqueous DSPM suspension experiments (1.50 ± 0.04‰, R^2 = 0.996). However, the ε^{202}Hg values for the aqueous WSDS experiments (1.35 ± 0.11‰, R^2 = 0.956 and 1.26 ± 0.11‰, R^2 = 0.948) were significantly smaller (p < 0.05) than that for the aqueous DSPM suspension experiments.

Although δ^{202}Hg values were strongly correlated with reaction extents when fitted using the Rayleigh model (R^2 > 0.95, see Table S4), as shown in Figure 2a, in many cases, calculated δ^{202}Hg values of the cumulative Hg(0) product are lower than model-fitted curves. For example, δ^{202}Hg values of the Hg(0) product for the soot aerosol experiment at an RH of 68% cross-fitted fractionation curves defined by ε^{202}Hg values of 1.75, 1.48, and 1.35 (‰). In fact, isotope enrichment factors calculated for individual time points varied progressively (see Table S6). In the soot aerosol experiment at an RH of 68%, for example, ε^{202}Hg values trended toward less positive values, from 1.81 to 1.40 (‰), as the reaction progressed [lower ln(f_R) values]. This trend, which was observed in all experimental results, indicates that the isotope fractionation factor decreased as the Hg(II) photoreduction reaction progressed, which may have resulted from different rates of reduction of Hg(II) in the two compartments identified in the kinetic analysis.

The fractionation of ^{199}Hg in the two aqueous-phase experiments also resulted in the enrichment of the heavier isotope (higher δ^{199}Hg) in the reactant. However, in the

https://doi.org/10.1021/acs.est.1c02679
Environ. Sci. Technol. 2021, 55, 13783−13791

aerosol-phase experiments, the remaining reactant Hg(II) became depleted in ^{199}Hg. As a result, for the aerosol-phase experiments, Δ^{199}Hg values of reactant Hg(II) decreased progressively as the reactions proceeded (Figure 2b and Table S2). In contrast, Δ^{199}Hg values of reactant Hg(II) in the aqueous-phase experiments (DSPM and WSDS) increased during the reduction of Hg(II). Reactant/product enrichment factors for ^{199}Hg (ε^{199}Hg) (Table S4) increased with water content from 28 to 100% in the aerosol and DSPM experiments and became even more positive in the WSDS experiments with only soluble soot components. Our results therefore show the unexpected finding that water content is a critical factor controlling not only the magnitude but also the direction of odd-MIF during the photoreduction of Hg(II) with soot aerosols. Toward the end of the DSPM and WSDS experiments, the direction of MIF changed sign (Figure 2b, Table S2). This is examined below.

Factors Contributing to Observed Hg Isotope Fractionation. Variation in MDF of Hg-stable isotopes in our diesel soot aerosol and aqueous-phase experiments can be explained based on the observed two-compartment kinetics of Hg(II) photoreduction. In the aerosol experiment with the lowest RH, the slow reacting form of Hg(II) in compartment 2 was dominant (91%) and Hg MDF was the highest. Increasing RH from 28 to 68% leads to a higher proportion of the fast reacting form of Hg(II) in compartment 1 (40%), a higher overall reduction rate and a lower extent of MDF than at low RH. The rate of Hg(II) photoreduction and the proportion of the fast reacting form of Hg(II) increased even more in experiments with soot suspensions and extracts, while the extent of MDF continued to decline (Table S4). These observations are consistent with theoretical and observed effects of reaction kinetics on MDF during kinetic fractionation.[31] The magnitude of mass-dependent Hg isotope fractionation during the photochemical reduction of Hg(II) with soot aerosols therefore depends on water content under the control of RH and temperature, which controls the relative abundances of two different forms of Hg(II) with different reaction rates. The coexistence of two forms of Hg(II) with different reaction rates on the aerosols, hypothesized soot particle-bound and dissolved forms of Hg(II), is consistent with our observation that within each experiment, isotope enrichment factors for MDF varied as the reactions proceeded.

Adsorption−desorption reactions may fractionate Hg-stable isotopes in both aerosol and aqueous phases. In our experiments, about 23% of total Hg(II) was present in the pre-equilibrated aqueous phase of the Hg(II)-DSPM suspension experiment prior to irradiation. As this was less than the fraction of total produced Hg(0), the desorption of Hg(II) from soot particles may have occurred as Hg(II) photoreduction progressed. Hg isotopic fractionation has been rarely studied in inhomogeneous systems. However, the adsorption/desorption of Hg(II) was shown to result in small extents of MDF (up to 0.62‰) and MIF (<0.1‰) of Hg isotopes.[26,46] Adsorption and/or desorption processes may therefore have affected MDF by at most 0.62‰[26,46] but probably had a limited effect on MIF in these experiments. While isotopic exchange due to aqueous-phase Hg(II)−Hg(0) equilibration has been observed in nonpurged, closed-system experiments,[28] such Hg isotope fractionation is unlikely to have exerted a major influence in our purged reactor experiments in which Hg(0) was continuously removed.

In both aerosol- and aqueous-phase experiments, Δ^{199}Hg was linearly correlated with Δ^{201}Hg ($R^2 > 0.97$ for all sets) and across all experiments, a Δ^{199}Hg/Δ^{201}Hg ratio of 1.15 ± 0.01 was obtained by linear regression (Figure S4). The Δ^{199}Hg/Δ^{201}Hg ratio we observed is similar to those previously reported (range of 1.19−1.31) for Hg(II) photoreduction in aqueous media with different Hg/DOC ratios.[39] In contrast, the thermal (non-photochemical) reduction of Hg(II) has a Δ^{199}Hg/Δ^{201}Hg ratio of 1.6, which has been linked to MIF arising from the nuclear volume effect.[47] This indicates that the magnetic isotope effect (MIE) dominated MIF observed in this study.

MIE arises from differences in the rates by which spin states of excited radical pairs undergo intersystem crossing (ISC) by hyperfine coupling in atoms with magnetic (odd mass) and nonmagnetic (even mass) nuclei.[48] Radical pairs with magnetic nuclei generated in the triplet state during photochemical reactions undergo ISC to the excited singlet state faster than radical pairs with nonmagnetic nuclei. The excited singlet-state radical pair can then recombine to form the original compound in the ground singlet state, thus increasing the ratio of odd isotopes in the reactant (for Hg, this is referred to as positive MIE). Radical pairs with magnetic nuclei initially in an excited singlet state will undergo ISC to an excited triplet faster than pairs with nonmagnetic nuclei and will dissociate into products leading to the depletion of odd isotopes in the reactant (negative MIE). Excited spin states and rates of ISC depend on the structure of the solvent cage surrounding radical pairs. Even at the lowest RH in our experiments, the soot aerosol particles would be coated with a layer of physically adsorbed liquid water.[49] Radical pairs of Hg(II) might then be surrounded by a solvent cage formed by water and perhaps functional groups on soot particle surfaces. For Hg(II), factors that affect the solvent cage are not entirely understood but include the coordinating ligand and pH.[50]

The odd-MIF of Hg isotopes we observed during the photochemical reduction of Hg(II) in the experiments with soot suspensions (DSPM, Δ^{199}Hg(II) up to 0.79‰) and extracts (WSDS, Δ^{199}Hg(II) up to 5.54‰) is similar to that reported previously for Hg(II) photoreduction with DOM in aquatic systems.[15,39,47] In those experiments, as in ours, reactant Hg(II) became enriched in ^{199}Hg as the reaction progressed and MIF was attributed to positive MIE. However, in our aerosol experiments, we observed enrichment of ^{199}Hg in the Hg(0) product, consistent with negative MIE. Negative MIF was observed during the photoreduction of Hg(II) complexed by reduced sulfur organic compounds (e.g., cysteine)[29,50] and Hg(II) accumulated by marine algae[51] and was attributed to the initial production of a singlet excited state of thiol-complexed Hg(II).[29,50] Thiols are present in soot,[52] and negative MIF may occur under conditions of low humidity when Hg(II) interacts primarily with surface sites on soot particles. Since the photochemical reduction of oxygen-complexed Hg(II) produces positive MIE,[29,50] with higher water content, Hg(II) may increasingly become complexed with hydroxide ions and water, rather than thiols, leading to greater extents of positive MIE.

Negative MIF was also observed by Sherman et al.[24] during Hg(II) photoreduction on Arctic snow. Sherman et al. hypothesized that the negative MIF they observed was due to multistep heterogeneous redox reactions occurring in the quasi-liquid surface layer of snow crystals.[24] Similar conditions exist on the surfaces of soot aerosols, which include a layer of

https://doi.org/10.1021/acs.est.1c02679
Environ. Sci. Technol. 2021, 55, 13783−13791

liquid water on the solid soot particles.[49] The amount of water associated with soot particle surfaces could alter the structure of the solvent cage surrounding Hg-ligand radical pairs, which in turn is expected to lead to changes in the rates of spin interconversion by ISC and the magnitude and direction of MIE.[48,53] In addition, the pH of the layer of liquid water covering soot particles would be controlled by acidic functional groups on soot particle surfaces.[54] In our aerosol experiments with low water content, low pH may have further altered the structure or polarity of the solvent cage[55] favoring the initial formation of singlet radical pairs and negative MIE, as observed by Motta et al.,[50] for Hg(II) complexed by sulfur or nitrogen ligands at low pH. As water content on soot particle surfaces increased with RH in our aerosol experiments, pH likely increased lowering the extent of negative MIE, leading ultimately in our aqueous-phase experiments to the initial formation of triplet radical pairs and positive MIE.

As was the case for δ^{202}Hg, differences between observations and fitted curves suggest that ^{199}Hg enrichment factors (ε^{199}Hg) estimated by Rayleigh model fits over all time points do not completely capture the effects of changes in the microscale chemical environments and multiple stages of Hg(II) photoreduction on odd-mercury isotope fractionation in our experiments. To better understand these differences, Δ^{199}Hg of the instantaneous Hg(0) product was plotted as a function of the fraction remaining (f_R, Figure 3). In our

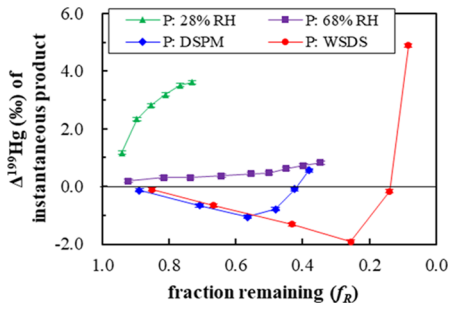

Figure 3. Measured Δ^{199}Hg values of the instantaneous product Hg(0) as a function of the fraction of the remaining Hg(II) ($f_R = 1 - Hg_{product}/Hg_{total}$) in soot aerosol- (RH 28 and 68%) and aqueous-phase (DSPM, WSDS) experiments.

aerosol-phase experiments, positive Δ^{199}Hg values of the instantaneous product increased progressively as the reactions proceeded. This indicates that the magnitude of negative MIF increased as the aerosol-phase reactions progressed, perhaps as a result of a continuous change in pH or other property of the water layer on soot particle surfaces (DOM concentration and viscosity) over time. In our aqueous-phase experiments, in contrast, negative Δ^{199}Hg values of the instantaneous product first decreased and then increased. Thus, there was a change in the direction of MIF in both aqueous-phase experiments. Interestingly, the change in the direction of MIF occurred after about 50% of Hg(II) had been reduced in the DSPM experiments and about 90% of Hg(II) had been reduced in the WSDS experiments. These fractions correspond to the sizes of compartment 1 in each case (51 and 95%, respectively) indicating that the photochemical reduction of aqueous-phase Hg(II) in compartment 1 resulted in positive MIF, while photochemical reduction of soot particle-bound Hg(II) in compartment 2 resulted in negative MIF. This provides additional evidence that the physical and chemical conditions associated with soot surface-bound Hg(II) favor the initial formation of a singlet radical pair and negative MIF during photochemical excitation, while aqueous complexes of Hg(II) with soot-derived soluble ligands initially produce a triplet radical pair and positive MIF.

In a recent study, photochemical reduction of Hg(II) with plant biochar-derived dissolved black carbon in aqueous-phase experiments resulted in no odd-MIF, while those with whole (non-demineralized) plant biochar-derived black carbon resulted in negative MIF.[56] Differences in the organic carbon source and conditions of production (temperature, oxygen content) of diesel soot and plant biochar may account for differences in the observed patterns of odd-MIF during the photoreduction of Hg(II) in the presence of these two materials. In addition, the presence of nitrate (from added mercuric nitrate) in the experiments with plant biochar black carbon may have resulted in the indirect photolysis of Hg(II) complexes by the reaction with nitrate-produced free radicals and negative-MIF due to the nuclear volume effect.[47]

Our results suggest that the rate of the photochemical reduction of Hg(II) associated with diesel soot particles is dominated by water-soluble components of soot and that the MDF and MIF of Hg isotopes vary with aerosol water content. The observed negative odd-MIF associated with dry soot aerosols could be important in environments with low RH such as deserts or at high altitude. Such areas may be a source of the reported significantly negative odd-MIF values of atmospheric particulate Hg in urban areas such as Beijing, China, where elevated levels of soot particles may exist due to residential, municipal, and commercial combustion activities.[33,34] In urban areas with higher humidity and where elevated levels of soot particles may exist due to residential, municipal, and commercial combustion activities, photochemical reduction of soot-bound Hg(II) would be expected to result in positive odd-MIF. Photoreduction of Hg(II) in high water content urban aerosols may, for example, contribute to generally higher Δ^{199}Hg values of fine aerosols collected in Beijing during the day than at night.[5] However, we should keep in mind that Hg isotope ratios in nature are dynamic and are affected by multiple sources and complex physicochemical processes, such as adsorption, oxidation, and volatilization. While the contributions of such processes to the isotope composition of atmospheric Hg are not fully characterized, the effects of such processes may be superimposed over those due to the photoreduction of Hg(II) in aerosols and surface waters. Therefore, we do not suggest applying our experimental results to natural conditions alone, as their effects on the fractionation of Hg isotopes in the environment should be evaluated together with other important processes.

■ ASSOCIATED CONTENT

Supporting Information

The Supporting Information is available free of charge at https://pubs.acs.org/doi/10.1021/acs.est.1c02679.

Additional experimental details including photoreactor design, Hg(II) photoreduction rates, Hg isotope composition (δ^{202}Hg) for duplicate Hg(II)-WSDS experiments, Δ^{199}Hg versus Δ^{201}Hg of the remaining Hg(II) and cumulative product Hg(0) for all samples, reacted fractions of Hg(II), measured and calculated isotope compositions of products and the remaining reactants, parallel pseudo-first-order rate model fits for

https://doi.org/10.1021/acs.est.1c02679
Environ. Sci. Technol. 2021, 55, 13783−13791

Hg(II) reduction, and Rayleigh model fits for MDF enrichment factors (PDF)

AUTHOR INFORMATION

Corresponding Author

John R. Reinfelder − *Department of Environmental Sciences, Rutgers University, New Brunswick 08901 New Jersey, United States;* orcid.org/0000-0002-3737-604X; Email: reinfeld@envsci.rutgers.edu

Authors

Qiang Huang − *State Key Laboratory of Environmental Geochemistry, Institute of Geochemistry, Chinese Academy of Sciences, Guiyang 550081 Guizhou, China; Department of Environmental Sciences, Rutgers University, New Brunswick 08901 New Jersey, United States;* orcid.org/0000-0003-1568-9042

Xiaoshuai He − *Department of Environmental Sciences, Rutgers University, New Brunswick 08901 New Jersey, United States*

Weilin Huang − *Department of Environmental Sciences, Rutgers University, New Brunswick 08901 New Jersey, United States*

Complete contact information is available at: https://pubs.acs.org/10.1021/acs.est.1c02679

Notes

The authors declare no competing financial interest.

ACKNOWLEDGMENTS

This study was supported financially by the National Key Research and Development Program of China (no. 2017YFC0212702), the National Natural Science Foundation of China (no. 41701268, 42077344), China Scholarship Council (201704910177), Opening Fund of the State Key Laboratory of Environmental Geochemistry (SKLEG2020202) and Guizhou Scientific Research Program (no. 20201Y167), and the U.S. National Science Foundation Chemical Oceanography Program (OCE-1634154). The authors sincerely thank the four anonymous reviewers for their constructive comments and suggestions and Dr. Linda Godfrey from the Department of Earth and Planetary Sciences, Rutgers University, for her assistance with the isotope measurements.

REFERENCES

(1) Ariya, P. A.; Amyot, M.; Dastoor, A.; Deeds, D.; Feinberg, A.; Kos, G.; Poulain, A.; Ryjkov, A.; Semeniuk, K.; Subir, M.; Toyota, K. Mercury physicochemical and biogeochemical transformation in the atmosphere and at atmospheric interfaces: A review and future directions. *Chem. Rev.* **2015**, *115*, 3760−3802.

(2) George, C.; Ammann, M.; D'Anna, B.; Donaldson, D. J.; Nizkorodov, S. A. Heterogeneous photochemistry in the atmosphere. *Chem. Rev.* **2015**, *115*, 4218−4258.

(3) Tong, Y.; Eichhorst, T.; Olson, M. R.; McGinnis, J. E.; Turner, I.; Rutter, A. P.; Shafer, M. M.; Wang, X.; Schauer, J. J. Atmospheric photolytic reduction of Hg(II) in dry aerosols. *Environ. Sci.: Processes Impacts* **2013**, *15*, 1883−1888.

(4) Deng, C.; Tong, Y.; Chen, L.; Yuan, W.; Sun, Y.; Li, J.; Wang, X.; Zhang, W.; Lin, H.; Xie, H.; Bu, X. Impact of particle chemical composition and water content on the photolytic reduction of particle-bound mercury. *Atmos. Environ.* **2019**, *200*, 24−33.

(5) Huang, Q.; Chen, J.; Huang, W.; Reinfelder, J. R.; Fu, P.; Yuan, S.; Wang, Z.; Yuan, W.; Cai, H.; Ren, H.; Sun, Y.; He, L. Diel variation in mercury stable isotope ratios records photoreduction of PM2.5-bound mercury. *Atmos. Chem. Phys.* **2019**, *19*, 315−325.

(6) de Foy, B.; Tong, Y.; Yin, X.; Zhang, W.; Kang, S.; Zhang, Q.; Zhang, G.; Wang, X.; Schauer, J. J. First field-based atmospheric observation of the reduction of reactive mercury driven by sunlight. *Atmos. Environ.* **2016**, *134*, 27−39.

(7) Si, L.; Ariya, P. Recent advances in atmospheric chemistry of mercury. *Atmosphere* **2018**, *9*, 76.

(8) Endo, S.; Grathwohl, P.; Haderlein, S. B.; Schmidt, T. C. Effects of native organic material and water on sorption properties of reference diesel soot. *Environ. Sci. Technol.* **2009**, *43*, 3187−3193.

(9) Monge, M. E.; D'Anna, B.; Mazri, L.; Giroir-Fendler, A.; Ammann, M.; Donaldson, D. J.; George, C. Light changes the atmospheric reactivity of soot. *Proc. Natl. Acad. Sci.* **2010**, *107*, 6605−6609.

(10) Bao, H.; Niggemann, J.; Luo, L.; Dittmar, T.; Kao, S.-J. Aerosols as a source of dissolved black carbon to the ocean. *Nat. Commun.* **2017**, *8*, 510.

(11) Li, M.; Bao, F.; Zhang, Y.; Song, W.; Chen, C.; Zhao, J. Role of elemental carbon in the photochemical aging of soot. *Proc. Natl. Acad. Sci.* **2018**, *115*, 7717−7722.

(12) Seigneur, C.; Abeck, H.; Chia, G.; Reinhard, M.; Bloom, N. S.; Prestbo, E.; Saxena, P. Mercury adsorption to elemental carbon (soot) particles and atmospheric particulate matter. *Atmos. Environ.* **1998**, *32*, 2649−2657.

(13) Hintelmann, H.; Lu, S. High precision isotope ratio measurements of mercury isotopes in cinnabar ores using multi-collector inductively coupled plasma mass spectrometry. *Analyst* **2003**, *128*, 635−639.

(14) Jackson, T. A.; Whittle, D. M.; Evans, M. S.; Muir, D. C. G. Evidence for mass-independent and mass-dependent fractionation of the stable isotopes of mercury by natural processes in aquatic ecosystems. *Appl. Geochem.* **2008**, *23*, 547−571.

(15) Bergquist, B. A.; Blum, J. D. Mass-dependent and -independent fractionation of Hg isotopes by photoreduction in aquatic systems. *Science* **2007**, *318*, 417−420.

(16) Chen, J.; Hintelmann, H.; Feng, X.; Dimock, B. Unusual fractionation of both odd and even mercury isotopes in precipitation from Peterborough, ON, Canada. *Geochim. Cosmochim. Acta* **2012**, *90*, 33−46.

(17) Gratz, L. E.; Keeler, G. J.; Blum, J. D.; Sherman, L. S. Isotopic composition and fractionation of mercury in Great Lakes precipitation and ambient air. *Environ. Sci. Technol.* **2010**, *44*, 7764−7770.

(18) Sherman, L. S.; Blum, J. D.; Keeler, G. J.; Demers, J. D.; Dvonch, J. T. Investigation of local mercury deposition from a coal-fired power plant using mercury isotopes. *Environ. Sci. Technol.* **2012**, *46*, 382−390.

(19) Jackson, T. A.; Muir, D. C. G.; Vincent, W. F. Historical variations in the stable isotope composition of mercury in Arctic Lake sediments. *Environ. Sci. Technol.* **2004**, *38*, 2813−2821.

(20) Yang, L.; Sturgeon, R. E. Isotopic fractionation of mercury induced by reduction and ethylation. *Anal. Bioanal. Chem.* **2009**, *393*, 377−385.

(21) Kritee, K.; Blum, J. D.; Johnson, M. W.; Bergquist, B. A.; Barkay, T. Mercury stable isotope fractionation during reduction of Hg(II) to Hg(0) by mercury resistant microorganisms. *Environ. Sci. Technol.* **2007**, *41*, 1889−1895.

(22) Estrade, N.; Carignan, J.; Sonke, J. E.; Donard, O. F. X. Mercury isotope fractionation during liquid-vapor evaporation experiments. *Geochim. Cosmochim. Acta* **2009**, *73*, 2693−2711.

(23) Ghosh, S.; Schauble, E. A.; Lacrampe Couloume, G.; Blum, J. D.; Bergquist, B. A. Estimation of nuclear volume dependent fractionation of mercury isotopes in equilibrium liquid−vapor evaporation experiments. *Chem. Geol.* **2013**, *336*, 5−12.

(24) Sherman, L. S.; Blum, J. D.; Johnson, K. P.; Keeler, G. J.; Barres, J. A.; Douglas, T. A. Mass-independent fractionation of mercury isotopes in Arctic snow driven by sunlight. *Nat. Geosci.* **2010**, *3*, 173−177.

(25) Smith, R. S.; Wiederhold, J. G.; Kretzschmar, R. Mercury isotope fractionation during precipitation of metacinnabar (β-HgS) and montroydite (HgO). *Environ. Sci. Technol.* **2015**, *49*, 4325−4334.
(26) Wiederhold, J. G.; Cramer, C. J.; Daniel, K.; Infante, I.; Bourdon, B.; Kretzschmar, R. Equilibrium mercury isotope fractionation between dissolved Hg(II) species and thiol-bound Hg. *Environ. Sci. Technol.* **2010**, *44*, 4191−4197.
(27) Janssen, S. E.; Schaefer, J. K.; Barkay, T.; Reinfelder, J. R. Fractionation of mercury stable isotopes during microbial methylmercury production by iron- and sulfate-reducing bacteria. *Environ. Sci. Technol.* **2016**, *50*, 8077−8083.
(28) Wang, Y.; Bartov, G.; Wang, T.; Reinfelder, J. R.; Johnson, T. M.; Yee, N. Rapid Attainment of Isotopic Equilibrium after Mercury Reduction by Ferrous Iron Minerals and Isotopic Exchange between Hg(II) and Hg(0). *ACS Earth Space Chem.* **2021**, *5*, 1384−1394.
(29) Zheng, W.; Hintelmann, H. Isotope fractionation of mercury during its photochemical reduction by low-molecular-weight organic compounds. *J. Phys. Chem. A* **2010**, *114*, 4246−4253.
(30) Sun, G.; Sommar, J.; Feng, X.; Lin, C.-J.; Ge, M.; Wang, W.; Yin, R.; Fu, X.; Shang, L. Mass-dependent and -independent fractionation of mercury isotope during gas-phase oxidation of elemental mercury vapor by atomic Cl and Br. *Environ. Sci. Technol.* **2016**, *50*, 9232−9241.
(31) Blum, J. D.; Sherman, L. S.; Johnson, M. W. Mercury isotopes in earth and environmental sciences. *Annu. Rev. Earth Planet. Sci.* **2014**, *42*, 249−269.
(32) Wiederhold, J. G. Metal stable isotope signatures as tracers in environmental geochemistry. *Environ. Sci. Technol.* **2015**, *49*, 2606−2624.
(33) Huang, Q.; Chen, J.; Huang, W.; Fu, P.; Guinot, B.; Feng, X.; Shang, L.; Wang, Z.; Wang, Z.; Yuan, S.; Cai, H.; Wei, L.; Yu, B. Isotopic composition for source identification of mercury in atmospheric fine particles. *Atmos. Chem. Phys.* **2016**, *16*, 11773−11786.
(34) Xu, H. M.; Sun, R. Y.; Cao, J. J.; Huang, R.-J.; Guinot, B.; Shen, Z. X.; Jiskra, M.; Li, C. X.; Du, B. Y.; He, C.; Liu, S. X.; Zhang, T.; Sonke, J. E. Mercury stable isotope compositions of Chinese urban fine particulates in winter haze days: Implications for Hg sources and transformations. *Chem. Geol.* **2019**, *504*, 267−275.
(35) Fu, X.; Zhang, H.; Feng, X.; Tan, Q.; Ming, L.; Liu, C.; Zhang, L. Domestic and transboundary sources of atmospheric particulate bound mercury in remote areas of China: Evidence from mercury isotopes. *Environ. Sci. Technol.* **2019**, *53*, 1947−1957.
(36) Rolison, J. M.; Landing, W. M.; Luke, W.; Cohen, M.; Salters, V. J. M. Isotopic composition of species-specific atmospheric Hg in a coastal environment. *Chem. Geol.* **2013**, *336*, 37−49.
(37) Decesari, S.; Facchini, M. C.; Matta, E.; Mircea, M.; Fuzzi, S.; Chughtai, A. R.; Smith, D. M. Water soluble organic compounds formed by oxidation of soot. *Atmos. Environ.* **2002**, *36*, 1827−1832.
(38) Song, J.; Li, M.; Jiang, B.; Wei, S.; Fan, X.; Peng, P. A. Molecular characterization of water-soluble humic like substances in smoke sarticles emitted from combustion of biomass materials and coal using ultrahigh-resolution electrospray ionization fourier transform ion cyclotron resonance mass spectrometry. *Environ. Sci. Technol.* **2018**, *52*, 2575−2585.
(39) Zheng, W.; Hintelmann, H. Mercury isotope fractionation during photoreduction in natural water is controlled by its Hg/DOC ratio. *Geochim. Cosmochim. Acta* **2009**, *73*, 6704−6715.
(40) Lu, Z.; MacFarlane, J. K.; Gschwend, P. M. Adsorption of organic compounds to diesel soot: Frontal analysis and polyparameter linear free-energy relationship. *Environ. Sci. Technol.* **2016**, *50*, 285−293.
(41) Reinfelder, J. R.; Janssen, S. E. Tracking legacy mercury in the Hackensack River estuary using mercury stable isotopes. *J. Hazard. Mater.* **2019**, *375*, 121−129.
(42) Huang, Q.; Liu, Y.; Chen, J.; Feng, X.; Huang, W.; Yuan, S.; Cai, H.; Fu, X. An improved dual-stage protocol to pre-concentrate mercury from airborne particles for precise isotopic measurement. *J. Anal. At. Spectrom.* **2015**, *30*, 957−966.
(43) Blum, J. D.; Bergquist, B. A. Reporting of variations in the natural isotopic composition of mercury. *Anal. Bioanal. Chem.* **2007**, *388*, 353−359.
(44) Sonke, J. E. A global model of mass independent mercury stable isotope fractionation. *Geochim. Cosmochim. Acta* **2011**, *75*, 4577−4590.
(45) Rose, C. H.; Ghosh, S.; Blum, J. D.; Bergquist, B. A. Effects of ultraviolet radiation on mercury isotope fractionation during photoreduction for inorganic and organic mercury species. *Chem. Geol.* **2015**, *405*, 102−111.
(46) Jiskra, M.; Wiederhold, J. G.; Bourdon, B.; Kretzschmar, R. Solution speciation controls mercury isotope fractionation of Hg(II) sorption to goethite. *Environ. Sci. Technol.* **2012**, *46*, 6654−6662.
(47) Zheng, W.; Hintelmann, H. Nuclear field shift effect in isotope fractionation of mercury during abiotic reduction in the absence of light. *J. Phys. Chem. A* **2010**, *114*, 4238−4245.
(48) Buchachenko, A. L. Magnetic isotope effect: Nuclear spin control of chemical reactions. *J. Phys. Chem. A* **2001**, *105*, 9995−10011.
(49) Popovicheva, O.; Persiantseva, N. M.; Shonija, N. K.; DeMott, P.; Koehler, K.; Petters, M.; Kreidenweis, S.; Tishkova, V.; Demirdjian, B.; Suzanne, J. Water interaction with hydrophobic and hydrophilic soot particles. *Phys. Chem. Chem. Phys.* **2008**, *10*, 2332−2344.
(50) Motta, L. C.; Kritee, K.; Blum, J. D.; Tsz-Ki Tsui, M.; Reinfelder, J. R. Mercury isotope fractionation during the photochemical reduction of Hg(II) coordinated with organic ligands. *J. Phys. Chem. A* **2020**, *124*, 2842−2853.
(51) Kritee, K.; Motta, L. C.; Blum, J. D.; Tsui, M. T.-K.; Reinfelder, J. R. Photomicrobial visible light-induced magnetic mass independent fractionation of mercury in a marine microalga. *ACS Earth Space Chem.* **2018**, *2*, 432−440.
(52) Liang, F.; Lu, M.; Birch, M. E.; Keener, T. C.; Liu, Z. Determination of polycyclic aromatic sulfur heterocycles in diesel particulate matter and diesel fuel by gas chromatography with atomic emission detection. *J. Chromatogr. A* **2006**, *1114*, 145−153.
(53) Turro, N. J.; Zhang, Z. Magnetic isotope and magnetic field effects on the product distributions of photolyses of dibenzyl ketone adsorbed on zeolites. *Tetrahedron Lett.* **1989**, *30*, 3761−3764.
(54) Chen, C.; Huang, W. Aggregation kinetics of diesel soot nanoparticles in wet environments. *Environ. Sci. Technol.* **2017**, *51*, 2077−2086.
(55) Saracino, G. A. A.; Tedeschi, A.; D'Errico, G.; Improta, R.; Franco, L.; Ruzzi, M.; Corvaia, C.; Barone, V. Solvent polarity and pH effects on the magnetic properties of Ionizable nitroxide radicals: A combined computational and experimental study of 2,2,5,5-tetramethyl-3-carboxypyrrolidine and 2,2,6,6-tetramethyl-4-carboxypiperidine nitroxides. *J. Phys. Chem. A* **2002**, *106*, 10700−10706.
(56) Li, L.; Wang, X.; Fu, H.; Qu, X.; Chen, J.; Tao, S.; Zhu, D. Dissolved black carbon facilitates photoreduction of Hg(II) to Hg(0) and reduces mercury uptake by lettuce (Lactuca sativa L.). *Environ. Sci. Technol.* **2020**, *54*, 11137−11145.

https://doi.org/10.1021/acs.est.1c02679
Environ. Sci. Technol. 2021, 55, 13783−13791